Physics and Imaging in Radiation Oncology 35 (2025) 100795

Contents lists available at ScienceDirect

Physics and Imaging in Radiation Oncology

journal homepage: www.sciencedirect.com/journal/physics-and-imaging-in-radiation-oncology

Original Research Article

Stability of liver position in a shuttle-based workflow for daily online magnetic resonance imaging-guided particle therapy☆

Friderike K. Longarino [a,b,c,*,1], Una Maguire [a,b,d,1], Cedric Beyer [b,c], Rita Pestana [b,c], Sebastian Regnery [b,c], Jürgen Debus [b,c,e,f], Sebastian Klüter [b,c], Katharina Seidensaal [b,c], Julia Bauer [b,c,f,g]

[a] Clinical Cooperation Unit Translational Radiation Oncology, German Cancer Research Center (DKFZ), Heidelberg, Germany
[b] Department of Radiation Oncology and Heidelberg Ion Beam Therapy Center (HIT), Heidelberg University Hospital, Heidelberg, Germany
[c] Heidelberg Institute for Radiation Oncology (HIRO), National Center for Radiation Research in Oncology (NCRO), Heidelberg, Germany
[d] School of Physics, University College Dublin, Dublin, Ireland
[e] Clinical Cooperation Unit Radiation Oncology, German Cancer Research Center (DKFZ), Heidelberg, Germany
[f] Medical Faculty, Heidelberg University, Heidelberg, Germany
[g] Department of Radiation Oncology, Charité – Universitätsmedizin Berlin, Corporate Member of Freie Universität Berlin and Humboldt-Universität zu Berlin, Berlin, Germany

ARTICLE INFO

Keywords:
MRI-guided particle therapy
Daily online adaptive radiotherapy
Shuttle transfer
Hepatocellular carcinoma

ABSTRACT

Background and Purpose: Online adaptive particle therapy makes it possible to consider interfractional changes during treatment, and therefore may lead to improved treatment outcomes. The advantages of online adaptive particle therapy may be realized with minimal workflow disruption by employing a shuttle-based daily quasi-online magnetic resonance imaging (MRI)-guided strategy, where the patient remains in the treatment position on a transfer table for MRI at a diagnostic device and subsequent treatment delivery. This study investigated potential liver displacement and deformation while using a shuttle-based workflow.
Material and methods: Fourteen healthy volunteers each underwent four MRI scans in a 1.5 T MRI scanner, with intra-hospital transport simulations between MRI scans. The study proceeded in the following steps: volunteer positioning, first MRI scan (MRI 1), ten-minute time control phase, second MRI scan (MRI 2), short transport phase, third MRI scan (MRI 3), long transport phase, and finally the last MRI scan (MRI 4). In each MRI set, the liver and relevant external outline were contoured. Dice similarity coefficient (DSC) and mean distance to agreement (MDA) were calculated to quantify consecutive shifts between image sets and accumulative shifts over the course of the study.
Results: Median MDA values for the liver (and for the external) contour were 0.6 mm (0.4 mm) for MRI 1 – MRI 2, 0.4 mm (0.5 mm) for MRI 2 – MRI 3, and 0.3 mm (0.7 mm) for MRI 3 – MRI 4. All subjects exhibited MDA values of <1.0 mm (<1.5 mm) and DSC values of >0.97 (>0.98) during transport phases. Outliers for the accumulative shift from MRI 1 – MRI 4 remained at <2.0 mm (<1.8 mm) after approximately 75 minutes.
Conclusions: The study demonstrated the high stability of the liver position in a shuttle-based workflow, a finding that can be used to enhance MRI-guided adaptive treatment strategies in radiotherapy.

1. Introduction

Particle therapy is one of the most advanced and precise forms of radiotherapy due to the favorable energy deposition and biological properties of charged particles [1]. However, successful application of particle therapy requires precise knowledge of the localization of the target and critical structures at the time of treatment [1,2]. Currently, image guidance is mainly based on 2D orthogonal X-ray imaging, in-

☆ This article is part of a special issue entitled: 'Online and real-time adaptive particle therapy' published in Physics and Imaging in Radiation Oncology.

* Corresponding author at: Clinical Cooperation Unit Translational Radiation Oncology, German Cancer Research Center (DKFZ), Im Neuenheimer Feld 280, 69120 Heidelberg, Germany.
E-mail address: f.longarino@dkfz-heidelberg.de (F.K. Longarino).

[1] These authors contributed equally to this work and share first authorship.

https://doi.org/10.1016/j.phro.2025.100795
Received 18 December 2024; Received in revised form 4 June 2025; Accepted 12 June 2025
Available online 14 June 2025

room 3D computed tomography (CT) imaging, on-board cone beam CT imaging, and surface tracking [3–5].

Integrating magnetic resonance imaging (MRI) with particle therapy has the potential to substantially improve treatment accuracy, particularly for patients whose cancers have substantial tumor motion or anatomical variation, and for those who are currently unable to receive safe dose escalation due to nearby critical structures [6]. Such MRI guidance makes it possible to control target localization on a daily basis, offering superior soft tissue contrast and no additional radiation dose compared to standard X-ray-based imaging [4,7]. It also enhances the possibilities for treatment plan adaptation. The feasibility of real-time MRI-guided photon therapy has been demonstrated [8], and recent advances in MRI-guided particle therapy show its potential to improve treatment by making it possible to target tumors more precisely and better avoid irradiating surrounding non-malignant tissues [4,6,7].

Despite these advancements, fully integrated, real-time MRI for particle therapy is still under development [4,6,9]. For interfractional changes, the benefits of MRI guidance can be realized by supplementing the current X-ray imaging approach with a shuttle-based daily quasi-online MRI-guided strategy [10]. This means that imaging and treatment are conducted with the patient remaining in the same position on a transfer table [11], which reduces workflow disruption and minimizes the risk of translational and/or rotational positional changes occurring during transfer from one system to the other [12–15].

Carbon ion radiotherapy in particular has exhibited the potential benefits of particle therapy for liver cancer, having demonstrated excellent local control for hepatocellular carcinoma without dose-limiting toxicity [16,17]. Integrating MRI into particle therapy may further enhance treatment outcomes by substantially reducing healthy liver toxicities in patients with liver tumors, even when the MRI is acquired outside of the treatment location [18]. Carbon ion radiotherapy of hepatocellular carcinoma, performed every other day in four fractions with high fraction doses of 10.5 Gy (biologically-weighted dose) [16], is a treatment scheme that requires adaptation. It therefore serves as a suitable initial case for the development and implementation of a shuttle-based MRI-guided adaptive workflow in particle therapy. The relocation of the patient from the MRI scanner, where initial imaging is conducted, to the treatment room poses a risk of organ displacement and deformation due to the passage of time and potential positional changes. A previous study concerning shuttle-based systems was conducted for relatively rigid body regions, such as the head and neck, with a focus on the reproducibility of positioning [15]. However, there is a lack of research regarding the anatomical robustness of a radiotherapy set-up in a shuttle-based workflow for the upper abdominal region. This region presents additional challenges due to its greater difficulty in precise positioning and its expected mobility during both the examination and transport processes.

This study investigated potential liver and external contour displacement and deformation in healthy volunteers while using a patient-transfer shuttle system for transport simulations of different expected durations and conditions. Such a shuttle system may enable a daily quasi-online MRI-guided adaptive treatment workflow for particle therapy and conventional photon radiotherapy.

2. Material and methods

2.1. Study design

The study design is illustrated in Fig. 1. Each volunteer was positioned in the liver stereotactic body radiotherapy (SBRT) immobilization set-up used clinically at the Heidelberg Ion Beam Therapy Center (HIT, Germany) on a vacuum mattress fixed to a transfer table (Slate AirShuttle) that can be transferred with an AirDrive Trolley (CQ Medical, Avondale, USA). The transfer device employs a low-friction air bearing to facilitate the transition of patients from the MRI scanner table to the treatment table without requiring any movement on the part of the patient [19]. The set-up comprised a bridge-based abdominal compression system (Diaphragm Control) to minimize breathing-related movement, a WingSTEP to position the volunteer's arms above the head, and a KneeSTEP for positioning of the legs (all components from IT-V, Innsbruck, Austria). The mean time required for the positioning was approximately twelve minutes.

Each volunteer underwent four MRI scans. Initial MRI (MRI 1) was performed to set a control for liver positioning. After this baseline MRI, the volunteer remained stationary in the MRI system for ten minutes to account for time-related positional changes (time control). Subsequently, a second set of MRI scans (MRI 2) was performed to evaluate any movement due solely to the passage of time. Next, the volunteer was transferred from the MRI table to the trolley on the transfer table. While still immobilized, the volunteer was then transported with the trolley via a typical intra-hospital transport route that involved traveling in a loop over smooth flooring and returning to the MRI system, to mimic the journey length and conditions from the MRI system to a treatment room within HIT (short transport of approximately five minutes including transfer time). A third set of MRI scans (MRI 3) was obtained to assess any liver displacement resulting from this simulated transport. For completeness, the volunteer was eventually transported around a longer loop which included travelling over uneven tiles to replicate more challenging journey conditions that might be encountered in other hospital settings (long transport of approximately eight minutes

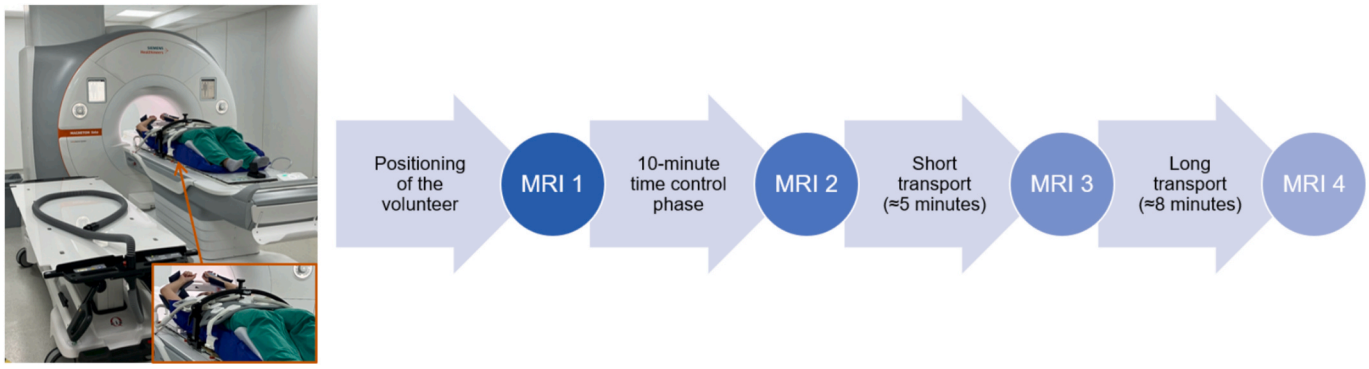

Fig. 1. Graphical representation of the study design. The subject was positioned on a vacuum mattress with abdominal compression on a transfer plate and subsequently transferred to the MRI table. A baseline series of MRI scans was taken (MRI 1). The subject remained stationary within the MRI scanner for a waiting period of ten minutes. A second set of MRI scans was then obtained (MRI 2). The subject, still immobilized, was transferred to the trolley, wheeled around a corridor to simulate the journey to the treatment room, and then transferred back to the MRI table. A third set of MRI scans was taken (MRI 3). The subject was transferred to the trolley, wheeled over uneven tiles to simulate a challenging, worst-case scenario of patient transport, and transferred back to the MRI table. A fourth set of MRI scans was taken (MRI 4).

including transfer time). A final set of MRI scans (MRI 4) was conducted post-simulation to evaluate potential liver displacement under these transport conditions. Overall, the mean total duration for the study was 87 minutes.

2.2. Study participants

Approval from the ethics committee of the Medical Faculty of Heidelberg University was obtained (S-964/2020). Fourteen healthy volunteers were enrolled, covering a range of ages and body mass indices (BMIs) (7 men, 7 women, median age: 29 years, range: 24–61 years, median height: 1.73 m, range: 1.62–1.90 m, median BMI: 22.8 kg/m^2, range: 19.8–32.9 kg/m^2). Written informed consent was obtained from each participant prior to MRI examination.

2.3. MR image acquisition

MR imaging was performed using a 1.5 T MAGNETOM Sola MRI scanner (Siemens Healthineers, Forchheim, Germany). The MRI scanner was situated in close proximity to the HIT treatment rooms, with the closest distance to the ion gantry being approximately 15 m [20]. For each set of scans, three MR pulse sequences were performed: a 3D T1 GRE (VIBE, TR: 6.8 ms, TE: 2.39/4.77 ms, spatial resolution: (1 × 1 × 3) mm^3, bandwidth: 470 Hz/pixel, acquisition time: 27 s), a respiratory-triggered 3D T2 TSE (SPACE, TR: 3000 ms, TE: 114 ms, spatial resolution: (1 × 1 × 3) mm^3, bandwidth: 723 Hz/pixel, acquisition time: 3 min and 18 s), and a respiratory self-gating 3D T1 Stack of Stars GRE (StarVIBE, TR: 5.7 ms, TE: 2.39 ms, spatial resolution: (1.7 × 1.7 × 3) mm^3, bandwidth: 560 Hz/pixel, binned into ten respiratory phases, acquisition time: 5 min and 11 s). The scan area completely covered the liver and its corresponding organ transitions and movement spaces.

2.4. Analysis of the liver MR images

In each of the four T2-weighted image sets (MRI 1 to MRI 4), the liver and the external outline for the region encompassing the liver were contoured by a physicist for each of the subjects by using RayStation version 11B (RaySearch Laboratories, Stockholm, Sweden). All scans were contoured by the same person to avoid inter-observer variability and verified by a radiation oncologist. Rigid registrations were performed between the four MRI scans. The Dice similarity coefficient (DSC) [21] and the mean distance to agreement (MDA) [22] were calculated using built-in RayStation functions [23,24]. Two primary sets of comparison were conducted for each subject: (i) comparing each scan with the initial scan to assess the accumulating total DSC and MDA throughout the study (accumulative shifts: MRI 1 – MRI 2, MRI 1 – MRI 3, MRI 1 – MRI 4); and (ii) comparing each scan with the subsequent scan to identify changes between consecutive image sets (consecutive shifts: MRI 1 – MRI 2, MRI 2 – MRI 3, MRI 3 – MRI 4). The mean and standard deviation of the DSC and MDA for the liver and the external contour were calculated for each comparison.

3. Results

All subjects tolerated the shuttle-based transfer and MR imaging well. Table 1 presents the mean and standard deviation of the DSC and MDA values found for the liver and the external contour for the fourteen subjects, facilitating comparison of the different MRI scans. Box plots summarizing the volunteer cohort are shown in Fig. 2, while subject specific values for all comparison scenarios are provided in Fig. 3 and 4. To visualize the difference in liver contour between MRI 1 and MRI 4, axial slices from three subjects are shown as examples (Fig. 5).

An overall downward trend in the DSC was observed across the study stages (accumulative shift) (Fig. 2(a)). This general trend is consistently reflected in a corresponding upward trend of MDA values over time (Fig. 2(c)). For the liver, the overall upward trend across the study stages (consecutive shift) of the DSC in Fig. 2(b) and of the corresponding downward trend of the MDA in Fig. 2(d) implies that there was more liver movement during the time control period than there was during the subsequent transport phases. The maximum MDA value attributable to the influence of time (MRI 1 – MRI 2) was 1.1 mm, which exceeded the maximum MDA value of 0.9 mm observed for the shuttle transfer (MRI 2 – MRI 3). As for consecutive shifts for the external contour, the time control (MRI 1 – MRI 2) had the highest DSC and lowest MDA values on average, followed by the short transport, and then the long transport (Fig. 2(b) and (d)). However, differences among participants were observed with respect to the impact of the waiting period, the short transport, and the long transport phase on the DSC and MDA values for the liver (Fig. 3(b) and (d)) and the external contour (Fig. 4(b) and (d)).

Table 1
Mean and standard deviation of the Dice similarity coefficient (DSC) and mean distance to agreement (MDA) for the liver and the external contour for the different comparisons.

Comparisons		Liver		External	
		DSC	MDA (mm)	DSC	MDA (mm)
Accumulative shift	MRI 1 – MRI 2	0.981 ± 0.006	0.6 ± 0.2	0.994 ± 0.003	0.4 ± 0.3
	MRI 1 – MRI 3	0.973 ± 0.009	0.9 ± 0.3	0.988 ± 0.006	0.9 ± 0.4
	MRI 1 – MRI 4	0.966 ± 0.013	1.1 ± 0.4	0.987 ± 0.007	1.0 ± 0.4
Consecutive shift	MRI 1 – MRI 2	0.981 ± 0.006	0.6 ± 0.2	0.994 ± 0.003	0.4 ± 0.3
	MRI 2 – MRI 3	0.984 ± 0.007	0.5 ± 0.2	0.992 ± 0.005	0.6 ± 0.4
	MRI 3 – MRI 4	0.988 ± 0.006	0.4 ± 0.2	0.991 ± 0.006	0.7 ± 0.4

In the following we report MDA and DSC values for the two analyzed structures, the liver and the external, with the results for the latter being provided in parentheses. For a clinically realistic scenario comparing MRI 2 and MRI 3, the median DSC and MDA values for the liver (and external) contour were observed to be 0.99 (0.99) and 0.4 mm (0.5 mm) (Fig. 2). Notably, for the liver (and external), all subjects exhibited DSC values of >0.97 (>0.98) and MDA values of <1 mm (<1.5 mm) during both transport phases. In the most unfavorable comparison between MRI 1 and MRI 4, the outliers remained for the liver (and external) at DSC >0.940 (>0.975) and MDA <2 mm (<1.8 mm).

4. Discussion

A shuttle-based MRI-guided approach offers the possibility of daily high soft tissue contrast control imaging while the patient remains in the treatment position. It is crucial to evaluate the stability of the patient immobilization in a shuttle-based workflow before such a workflow can be clinically implemented, since any displacement or deformation can compromise treatment outcomes. Our study demonstrated that the liver SBRT immobilization set-up is suitable to achieve a high stability of the liver position under various transport conditions.

The maximum MDA attributable to the influence of time (ten-minute waiting period plus about five-minute scanning for different MRI sequences) was 1.1 mm for the liver, which exceeded the maximum MDA value observed after a shuttle transfer (Fig. 2). For both, the liver and the external, a high geometric stability was observed in the two analyzed measures (MDA and DSC) for all subjects during the short and the long shuttle transfer periods. Specifically, for the liver (and external), all subjects exhibited DSC values of >0.97 (>0.98) and MDA values of <1.0 mm (<1.5 mm) during both the short and long shuttle transfer periods (Fig. 2). This demonstrates the robustness of the shuttle-based workflow. Observed MDA values were in the order of the MR image

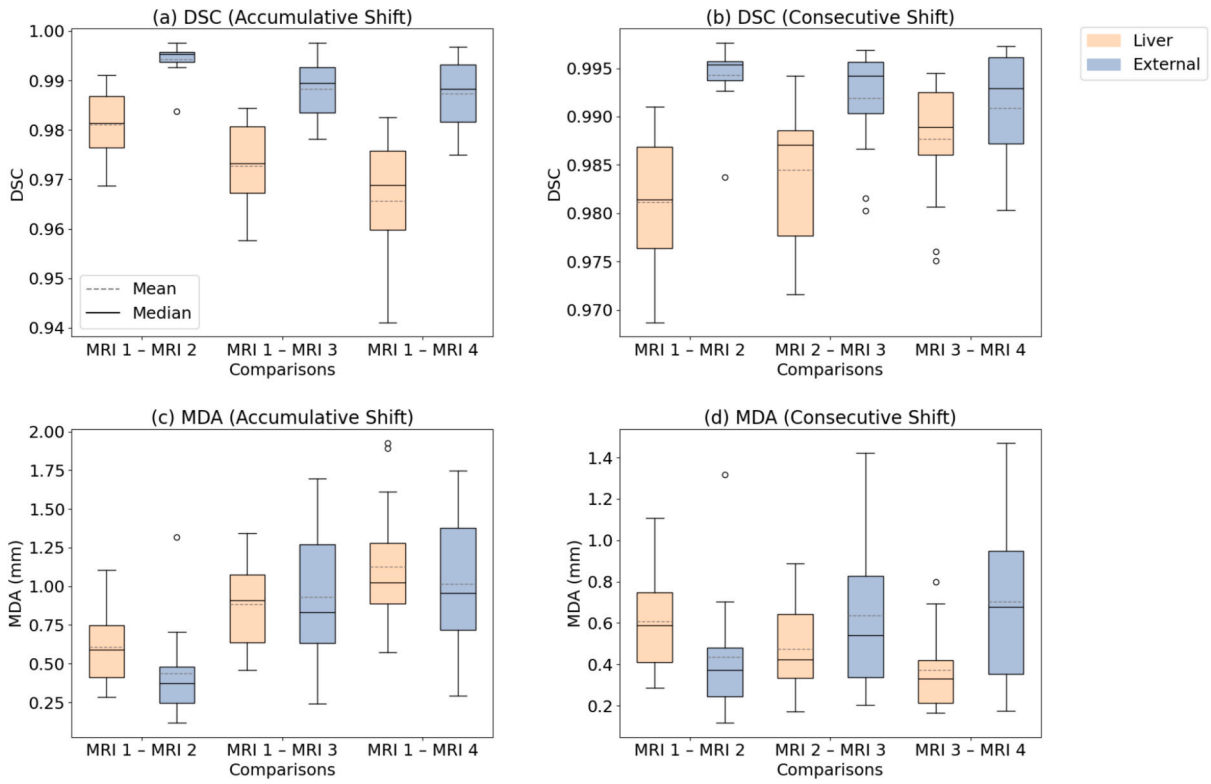

Fig. 2. Box plots showing the distribution of the Dice similarity coefficient (DSC) (a, b) and mean distance to agreement (MDA) values (c, d) for the liver and the external contour for the different comparisons. On each box, the central solid line (black) indicates the median, the dotted line (gray) indicates the mean, and the bottom and top edges of the box indicate the 25th and 75th percentiles, respectively. The whiskers extend to the most extreme data points (i.e., smallest observation ≥lower quartile – 1.5 × interquartile range, and largest observation ≤upper quartile + 1.5 × interquartile range), and the outliers are plotted individually using a circle symbol. Box plots comparing the accumulative shift are shown in (a) and (c). Box plots comparing the consecutive shift are shown in (b) and (d).

resolution and considerably smaller than the overall uncertainty margins of 5–7 mm currently applied for carbon ion radiotherapy of hepatocellular carcinoma [16]. Even after one hour and two shuttle transports, the outliers for the liver (and external) remained at DSC >0.940 (>0.975) and MDA <2.0 mm (<1.8 mm) (Fig. 2). Analysis indicated no discernible trends linking the variations in DSC and MDA to sex, age, or BMI, which implies that these demographic factors did not affect the study outcomes. However, the small size of the volunteer group means that these findings may need to be validated in larger cohorts. The DSC and MDA values obtained in this study were within the tolerances published by the American Association of Physicists in Medicine (AAPM) Task Group No. 132, which recommends DSC values above 0.8 and MDA values below 3 mm when evaluating image registrations in photon therapy [25]. At the time of writing, no analogous DSC and MDA guideline values exist for particle therapy. MDA values of less than 1 mm in the liver contour, as were observed in the shuttle transfer periods in this study, may be considered acceptable for carbon ion SBRT in cases of liver cancer.

At HIT, the immobilization set-up currently employed for carbon ion liver SBRT patients is similar to the one utilized in this study; this set-up comprises a vacuum mattress, a bridge-based abdominal compression system, an arm holder, and a knee support (Fig. 1). In liver cancer patients receiving carbon ion radiotherapy, SBRT is generally carried out with one or two beams [17], with beam paths selected to avoid passing through the abdominal compression system. In the shuttle-based workflow, the patient is immobilized on a transfer table, receives daily MRI at 1.5 T to verify patient positioning (3D) and residual respiratory motion of the target (4D), and is then transferred to the treatment room and placed onto the treatment couch. The total duration of the shuttle-based workflow is approximately 20 minutes, including 15 minutes of MRI time and 5 minutes of transfer time. Currently, in-room CT imaging at the horizontal beamline is still used for liver position verification and fast dose forward calculation of the treatment plan; however, research is being conducted to replace this step with MRI so that the workflow can be utilized for control imaging for the gantry beamline, which may enable new treatment options. The patient positioning is subsequently verified with planar in-room X-ray imaging, which is available at both the horizontal and gantry beamline. The implementation of a shuttle-based workflow for online adaptive particle therapy makes it possible to consider interfractional changes during treatment, which may lead to improved treatment outcomes compared to non-adaptive or occasional offline adaptive treatments [6,11,26,27]. The integration of a shuttle system with an MRI scanner situated outside the treatment room thus represents a flexible and cost-effective alternative to fully integrated MRI-guided radiotherapy systems, which are not yet commercially available for particle therapy [9]. Additionally, the shuttle-based system can be utilized to transport patients between the CT and MRI systems, which could further reduce uncertainty between the planning CT and planning MRI. The robustness of the immobilization set-up observed in our study for the different transport scenarios is a promising starting point for such integration.

The results of this study align with those of a previous study involving twenty patients with pelvic malignancies, which indicated a median positional difference between MR and CBCT imaging based on fiducial matching of ≤2 mm in all spatial directions when using a shuttle system [14].

The findings of this study showed that, overall, ten out of fourteen subjects exhibited a lower DSC and higher MDA for the comparisons between MRI 2 and MRI 3 than between MRI 3 and MRI 4 (Fig. 3). This suggests that the duration and conditions of the transport do not have a substantial impact on the robustness of the workflow. However, the subjects' own movements may have affected the result. When MR

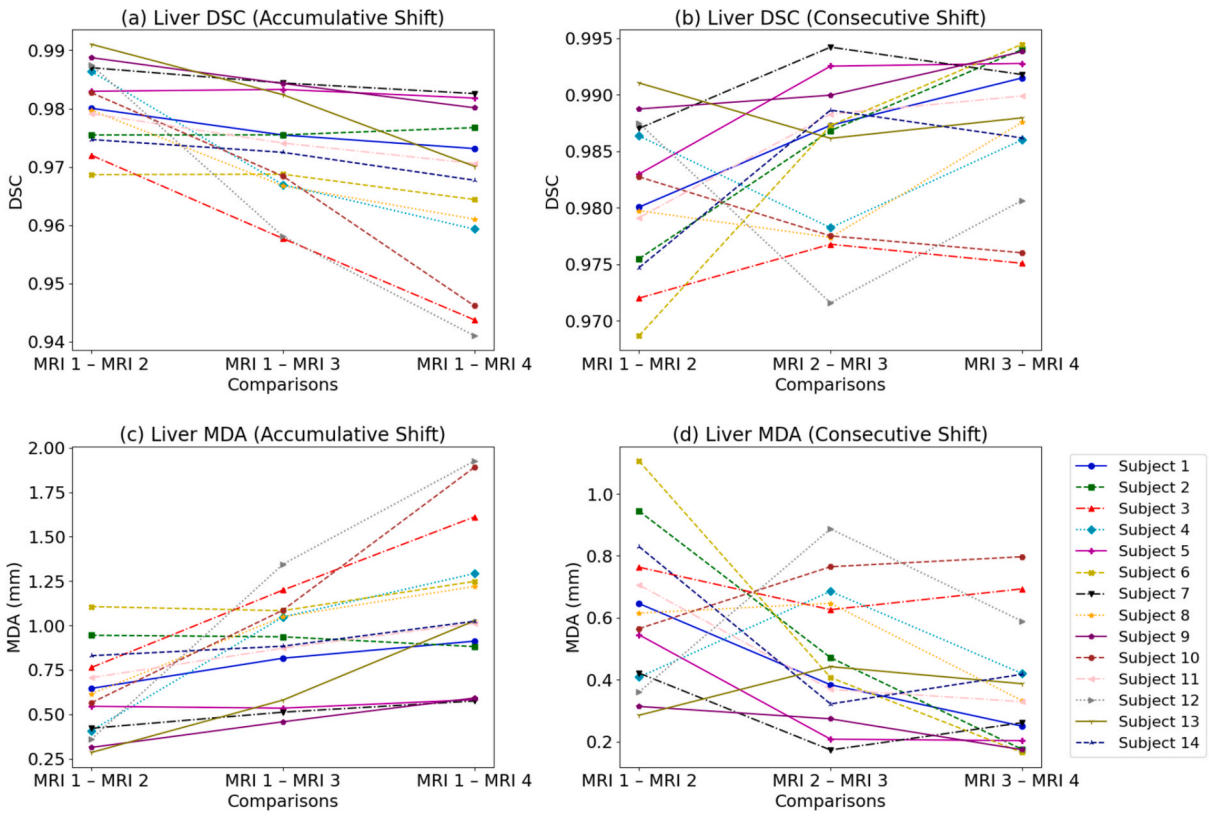

Fig. 3. Line graphs showing the Dice similarity coefficient (DSC) (a, b) and the mean distance to agreement (MDA) values (c, d) for the liver contour for each subject for the different comparisons. Line graphs comparing the accumulative shift are shown in (a) and (c). Line graphs comparing the consecutive shift are shown in (b) and (d).

images were not being acquired, volunteers were permitted to move and stretch their arms to alleviate the discomfort of holding them above their heads. At the start of the short transport phase between MRI 2 and MRI 3, volunteers had already been stationary for about 35 minutes, which prompted them to stretch more than during the long transport phase, which followed directly on MRI 3, during which they had been stationary for only about 13 minutes. This behavioral variance could account for the trend observed in the data. It is also conceivable that the position of the liver becomes stabilized over time due to the volunteers becoming more relaxed. Moreover, the difference between MRI 1 and MRI 2 could also be caused by liver drift due to a change in the direction of the gravitational force between standing and supine position [28].

Furthermore, during the contouring of the scans, it was observed that most movement occurred in the lower right lobe of the liver, which was likely influenced by the deformation and positional changes of the gall bladder and intestines. Notably, volunteers were given no instructions about dietary restrictions prior to scanning, and the total study duration for each subject was about 90 minutes. This timeframe is significant enough for previously consumed food to progress substantially through the digestive system [29]. The gradual process of digestion may have introduced an internal source of movement of the liver, caused by the expansion and contraction of the intestines and gall bladder.

Specific issues arose with individual subjects during the study that may have contributed to variability in the data. For instance, during the study of subject 12, the abdominal compression device was dislodged and had to be reapplied during the transfer of the volunteer from the MRI table to the trolley. The subject was not excluded from the study because this represents a worst-case scenario. The analysis demonstrated that even under these unfavorable conditions, the liver position remained highly stable in the shuttle-based workflow. Additionally, during the study of subject 4, it was determined that the vacuum mattress was not adequately tight around the torso, which made it possible for the volunteer to move more than was desirable. Nevertheless, in these instances, the MDA values remained below 1 mm during the transport simulations.

The strengths and limitations of the study can be summarized as follows.

This study was a systematic investigation, which quantified liver movement related to both time and the transport scenarios employed. Our approach provided clear insights into how different conditions affect the stability of the liver position in a shuttle-based workflow, and demonstrated the high anatomical robustness of such a set-up. Additionally, the inclusion of fourteen healthy volunteers, involving both men and women of various ages and BMIs, enhanced the generalizability of the results. This diverse participant profile allowed for a more comprehensive assessment of liver movement across different demographics. Furthermore, the incorporation of both short and long shuttle transport scenarios illustrated the system's potential adaptability, which suggests that these findings may be applicable to other hospital settings with similar transport conditions. The study also simulated a realistic patient scenario by not imposing dietary restrictions prior to MR imaging, which strengthens the applicability of the findings to typical patient situations.

While the cohort included fourteen healthy volunteers, this relatively small sample size limits the statistical power of the findings. Further research involving larger patient populations is needed to validate the results and assess their clinical applicability. The exclusive use of healthy volunteers also presents a limitation, since the biomechanical responses and liver positioning may differ in patients diagnosed with cancer. A further limitation is that, with healthy volunteers, it is not possible to assess the stability of a target volume. Given the smaller size of target volumes, they may be more sensitive than the entire liver.

Future research should consider expanding the investigation to other treatment locations, such as the pancreas or pelvis, to assess whether the

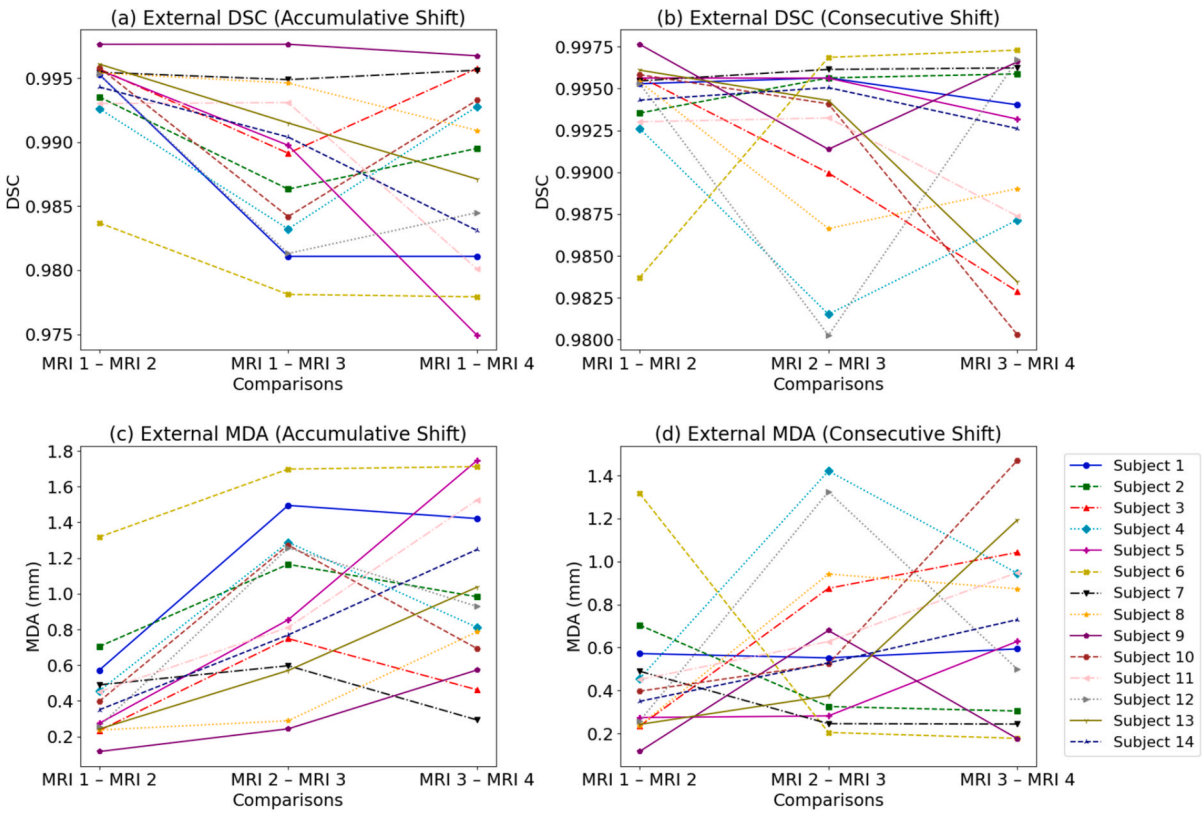

Fig. 4. Line graphs showing the Dice similarity coefficient (DSC) (a, b) and the mean distance to agreement (MDA) values (c, d) for the external contour for each subject for the different comparisons. Line graphs comparing the accumulative shift are shown in (a) and (c). Line graphs comparing the consecutive shift are shown in (b) and (d).

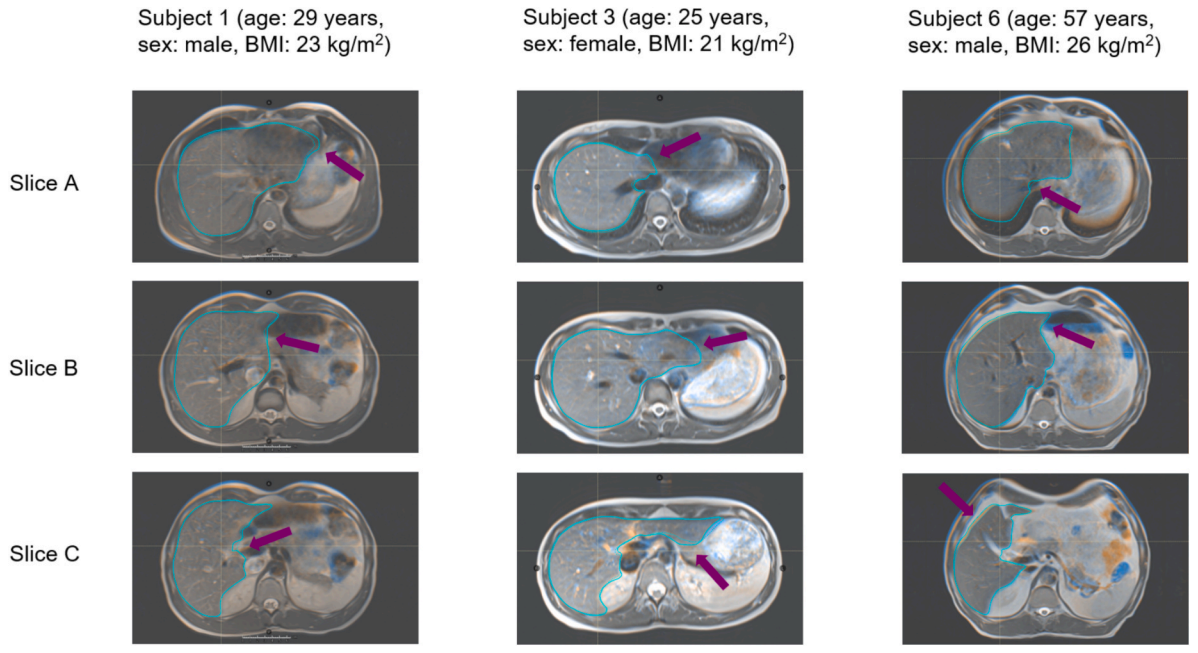

Fig. 5. Three axial slices from subject 1 (DSC: 0.97, MDA: 0.9 mm), subject 3 (DSC: 0.94, MDA: 1.6 mm), and subject 6 (DSC: 0.96, MDA: 1.2 mm) are presented to show the difference in liver contour between MRI 1 (solid line) and MRI 4 (dotted line). Arrows indicate differences in liver contour.

findings regarding liver positioning stability and transport workflow are applicable to other anatomical sites. Furthermore, future studies might benefit from exploring alternative abdominal compression systems that may expand patient eligibility. It is also essential to conduct subsequent research involving actual patients to further validate and extend the applicability of the current findings, since the responses of healthy volunteers may not entirely reflect the complexities of cancer patients. Additionally, implementing dietary instructions specifying what to eat or avoid prior to MR imaging could help standardize conditions and minimize variability in liver positioning caused by factors such as

digestion and abdominal distension.

In summary, the study demonstrated that a high stability of the liver position can be ensured during a shuttle-based workflow for daily quasi-online MRI-guided adaptive particle therapy. The observed metrics, including an MDA of less than 1 mm and a DSC exceeding 0.97 for the livers of all participants during various transport simulations, underscore the anatomical robustness of this workflow for high-precision particle therapy. Accordingly, the shuttle-based workflow provides a valuable opportunity to enhance MRI-guided adaptive treatment strategies in particle therapy and conventional photon radiotherapy.

CRediT authorship contribution statement

Friderike K. Longarino: Conceptualization, Data curation, Formal analysis, Investigation, Methodology, Software, Visualization, Writing – original draft, Writing – review & editing. **Una Maguire:** Formal analysis, Funding acquisition, Investigation, Methodology, Software, Visualization, Writing – original draft, Writing – review & editing. **Cedric Beyer:** Data curation, Investigation, Methodology, Writing – review & editing. **Rita Pestana:** Methodology, Software, Writing – review & editing. **Sebastian Regnery:** Methodology, Writing – review & editing. **Jürgen Debus:** Funding acquisition, Writing – review & editing. **Sebastian Klüter:** Project administration, Writing – review & editing. **Katharina Seidensaal:** Conceptualization, Methodology, Resources, Supervision, Writing – review & editing. **Julia Bauer:** Conceptualization, Methodology, Resources, Supervision, Writing – review & editing.

Declaration of competing interest

The authors declare the following financial interests/personal relationships which may be considered as potential competing interests: JD reports a relationship that includes funding grants with the following: RaySearch Laboratories AB, Vision RT Ltd, Merck Serono GmbH, Siemens Healthcare GmbH, PTW-Freiburg Dr Pychlau GmbH, Accuray Inc. JD reports a relationship with IntraOp that includes nonfinancial support.

The other authors declare that they have no known competing financial interests or personal relationships that could have appeared to influence the work reported in this paper.

Acknowledgments

This work was kindly supported by the German Federal Ministry of Research, Technology and Space within the funding program “Adaptive radiotherapy with MR guided ion beams” (ARTEMIS, 13GW0436A). Una Maguire gratefully acknowledges support from the German Academic Exchange Service (DAAD).

References

[1] Durante M, Flanz J. Charged particle beams to cure cancer: Strengths and challenges. Semin Oncol 2019;46:219–25. https://doi.org/10.1053/j.seminoncol.2019.07.007.
[2] Paganetti H, Botas P, Sharp GC, Winey B. Adaptive proton therapy. Phys Med Biol 2021;66:22TR01. https://doi.org/10.1088/1361-6560/ac344f.
[3] Landry G, Hua CH. Current state and future applications of radiological image guidance for particle therapy. Med Phys 2018;45:e1086–95. https://doi.org/10.1002/mp.12744.
[4] Hoffmann A, Oborn B, Moteabbed M, Yan S, Bortfeld T, Knopf A, et al. MR-guided proton therapy: a review and a preview. Radiat Oncol 2020;15:129. https://doi.org/10.1186/s13014-020-01571-x.
[5] Lane SA, Slater JM, Yang GY. Image-guided proton therapy: a comprehensive review. Cancers 2023;15:2555. https://doi.org/10.3390/cancers15092555.
[6] Pham TT, Whelan B, Oborn BM, Delaney GP, Vinod S, Brighi C, et al. Magnetic resonance imaging (MRI) guided proton therapy: a review of the clinical challenges, potential benefits and pathway to implementation. Radiother Oncol 2022;170:37–47. https://doi.org/10.1016/j.radonc.2022.02.031.
[7] Keall PJ, Brighi C, Glide-Hurst C, Liney G, Liu PZY, Lydiard S, et al. Integrated MRI-guided radiotherapy — opportunities and challenges. Nat Rev Clin Oncol 2022;19:458–70. https://doi.org/10.1038/s41571-022-00631-3.
[8] Otazo R, Lambin P, Pignol JP, Ladd ME, Schlemmer H-P, Baumann M, et al. MRI-guided radiation therapy: an emerging paradigm in adaptive radiation oncology. Radiology 2021;298:248–60. https://doi.org/10.1148/radiol.2020202747.
[9] Herrick M, Penfold S, Santos A, Hickson K. A systematic review of volumetric image guidance in proton therapy. Phys Eng Sci Med 2023;46:963–75. https://doi.org/10.1007/s13246-023-01294-9.
[10] Bauer J, Beyer C, Dorsch S, Ellerbrock M, Hansmann T, Klüter S, et al. Towards daily online MR-image-guided particle therapy: first clinical application of a shuttle-based workflow at the Heidelberg Ion-Beam Therapy Center. Int J Part Ther 2024;12(Supplement):100243. https://doi.org/10.1016/j.ijpt.2024.100243.
[11] Albertini F, Matter M, Nenoff L, Zhang Y, Lomax A. Online daily adaptive proton therapy. Br J Radiol 2020;93:20190594. https://doi.org/10.1259/bjr.20190594.
[12] Bolsi A, Lomax AJ, Pedroni E, Goitein G, Hug E. Experiences at the Paul Scherrer Institute with a remote patient positioning procedure for high-throughput proton radiation therapy. Int J Radiat Oncol Biol Phys 2008;71:1581–90. https://doi.org/10.1016/j.ijrobp.2008.02.079.
[13] Bostel T, Nicolay NH, Grossmann JG, Mohr A, Delorme S, Echner G, et al. MR-guidance – a clinical study to evaluate a shuttle- based MR-linac connection to provide MR-guided radiotherapy. Radiat Oncol 2014;9:12. https://doi.org/10.1186/1748-717X-9-12.
[14] Bostel T, Pfaffenberger A, Delorme S, Dreher C, Echner G, Haering P, et al. Prospective feasibility analysis of a novel off-line approach for MR-guided radiotherapy. Strahlenther Onkol 2018;194:425–34. https://doi.org/10.1007/s00066-017-1258-y.
[15] Zhou Y, Yuan J, Wong OL, Fung WWK, Cheng KF, Cheung KY, et al. Assessment of positional reproducibility in the head and neck on a 1.5-T MR simulator for an offline MR-guided radiotherapy solution. Quant Imaging Med Surg 2018;8:925–35. https://doi.org/10.21037/qims.2018.10.03.
[16] Hoegen-Saßmannshausen P, Naumann P, Hoffmeister-Wittmann P, Harrabi SB, Seidensaal K, Weykamp F, et al. Carbon ion radiotherapy of hepatocellular carcinoma provides excellent local control: the prospective phase I PROMETHEUS trial. JHEP Rep 2024;6:101063. https://doi.org/10.1016/j.jhepr.2024.101063.
[17] Hoffmeister-Wittmann P, Hoegen-Saßmannshausen P, Wicklein L, Weykamp F, Seidensaal K, Springfeld C, et al. Stereotactic body radiotherapy with carbon ions as local ablative treatment in patients with primary liver cancer. Radiat Oncol 2025;20:23. https://doi.org/10.1186/s13014-025-02594-y.
[18] Moteabbed M, Smeets J, Hong TS, Janssens G, Labarbe R, Wolfgang JA, et al. Toward MR-integrated proton therapy: modeling the potential benefits for liver tumors. Phys Med Biol 2021;66:195004. https://doi.org/10.1088/1361-6560/ac1ef2.
[19] Kim J-Y, Tawk B, Knoll M, Hoegen-Saßmannshausen P, Liermann J, Huber PE, et al. Clinical workflow of cone beam computer tomography-based Daily online adaptive radiotherapy with offline magnetic resonance guidance: the modular adaptive radiotherapy system (MARS). Cancers 2024;16:1210. https://doi.org/10.3390/cancers16061210.
[20] Dorsch S, Paul K, Beyer C, Karger CP, Jäkel O, Debus J, et al. Quality assurance and temporal stability of a 1.5 T MRI scanner for MR-guided photon and particle therapy. Z Med Phys 2025;35:204–17. https://doi.org/10.1016/j.zemedi.2023.04.004.
[21] Dice LR. Measures of the amount of ecologic association between species. Ecology 1945;26:297–302. https://doi.org/10.2307/1932409.
[22] Chalana V, Kim Y. A methodology for evaluation of boundary detection algorithms on medical images. IEEE Trans Med Imaging 1997;16:642–52. https://doi.org/10.1109/42.640755.
[23] Janson M, Glimelius L, Fredriksson A, Traneus E, Engwall E. Treatment planning of scanned proton beams in RayStation. Med Dosim 2024;49:2–12. https://doi.org/10.1016/j.meddos.2023.10.009.
[24] Pestana R, Seidensaal K, Beyer C, Debus J, Klüter S, Bauer J. Evaluation of pelvic MRI-to-CT deformable registration for adaptive MR-guided particle therapy. Int J Part Ther 2024;14:100636. https://doi.org/10.1016/j.ijpt.2024.100636.
[25] Brock KK, Mutic S, McNutt TR, Li Hua, Kessler ML. Use of image registration and fusion algorithms and techniques in radiotherapy: report of the AAPM Radiation Therapy Committee Task Group No. 132. Med Phys 2017;44:e43–76. https://doi.org/10.1002/mp.12256.
[26] Albertini F, Czerska K, Vazquez M, Andaca I, Bachtiary B, Besson R, et al. First clinical implementation of a highly efficient daily online adapted proton therapy (DAPT) workflow. Phys Med Biol 2024;69:215030. https://doi.org/10.1088/1361-6560/ad7cbd.
[27] Regnery S, Pestana R, Hoffmeister-Wittmann P, Mielke T, Hoegen-Saßmannshausen P, Weykamp F, et al. Image-guided carbon ion stereotactic radiotherapy of hepatocellular carcinoma: paving the way for MR-guided online adaptive therapy. Radiother Oncol 2025;206:S1770–2. https://doi.org/10.1016/S0167-8140(25)00458-X.
[28] von Siebenthal M, Székely G, Lomax AJ, Cattin PC. Systematic errors in respiratory gating due to intrafraction deformations of the liver. Med Phys 2007;34:3620–9. https://doi.org/10.1118/1.2767053.
[29] Hellmig S, Von Schöning F, Gadow C, Katsoulis S, Hedderich J, Fölsch UR, et al. Gastric emptying time of fluids and solids in healthy subjects determined by 13C breath tests: Influence of age, sex, and body mass index. J Gastroenterol Hepatol 2006;21:1832–8. https://doi.org/10.1111/j.1440-1746.2006.04449.x.